AIAA JOURNAL
Vol. 43, No. 9, September 2005

Control of Sublayer Streaks Using Microjet Actuators

Duncan A. Lockerby*
Brunel University, Uxbridge, England UB8 3PH, United Kingdom
Peter W. Carpenter†
University of Warwick, Coventry, England CV4 7AL, United Kingdom
and
Christopher Davies‡
Cardiff University, Cardiff, Wales CF24 4AG, United Kingdom

A combination of numerical techniques is employed to model the interaction of a microjet actuator and the near-wall coherent structures found in turbulent boundary layers. These streak-like flow structures are modeled by using an analogy between them and Klebanoff modes. The Klebanoff mode can be modeled by seeking an optimum response within a Blasius boundary layer to a freestream streamwise vorticity source generated by an applied body force. In a similar way, except that a turbulent mean-velocity profile is used and the streamwise vorticity source is now located within the boundary layer, sublayer streaks can be generated. The results of these simulations agree well with previous experimental and numerical observations of streak dynamics and structure. The linear models of the streak and boundary layer are combined to simulate the basic realization of streak control using microjet actuation. It is concluded that to increase turbulence production, low-speed streaks should be targeted, and to decrease it high-speed streaks should be targeted. Spanwise and streamwise arrays of actuators are studied and found to be more effective than isolated actuators. In particular, a streamwise array of smaller actuators is found to be much more effective than a single larger actuator producing the same mass flow as the actuator array. A coupled simulation of the actuator, streak, and boundary layer is performed. The intensification of a low-speed streak is demonstrated. The pressure footprint of the convecting streak can have a significant influence on the output velocity of a microjet. This suggests that the weak microjets might respond violently and unpredictably to the nondeterministic pressure fluctuations of the turbulent boundary layer.

Nomenclature

a	=	parameter specifying streamwise width of impulsive body force
b	=	parameter specifying wall-normal width of impulsive body force
$\boldsymbol{F}$	=	fictitious body force
G	=	amplitude of body force
$\boldsymbol{N}$	=	$\bar{\boldsymbol{\Omega}} \times \bar{\boldsymbol{U}} + \boldsymbol{\omega} \times \bar{\boldsymbol{U}} + \boldsymbol{N}'$
$\boldsymbol{N}'$	=	$\boldsymbol{\omega} \times \boldsymbol{u}$
N_c	=	number of Chebyshev polynomials
N_f	=	number of spanwise Fourier modes
Re	=	Reynolds number, $U_\infty \delta^* / \nu$
r	=	radius of microjet orifice, m
t	=	dimensionless time
t_p	=	dimensionless period of microjet actuation
U_∞	=	freestream velocity, m s^{-1}
$\bar{U}$	=	dimensionless mean velocity profile
u	=	dimensionless streamwise velocity perturbation
v	=	dimensionless wall-normal velocity perturbation
v^*	=	friction velocity, m s^{-1}
V_c	=	dimensionless centerline velocity of microjet actuation
V_m	=	maximum dimensionless velocity of microjet actuation
w	=	dimensionless spanwise velocity perturbation
x	=	dimensionless streamwise coordinate
x_f, z_f	=	dimensionless coordinates of body-force location
y	=	dimensionless spanwise coordinate
z	=	dimensionless wall-normal coordinate
β	=	dimensionless spanwise wave number
Δt	=	dimensionless time step
Δx	=	streamwise grid spacing
δ^*	=	boundary-layer displacement thickness, m
λ	=	dimensionless spanwise wavelength
ν	=	kinematic viscosity, m^2 s^{-1}
$\bar{\boldsymbol{\Omega}}$	=	dimensionless mean vorticity
$\boldsymbol{\omega}$	=	dimensionless vorticity perturbation
ω_x	=	dimensionless streamwise vorticity perturbation
ω_y	=	dimensionless spanwise vorticity perturbation
ω_z	=	dimensionless wall-normal vorticity perturbation

Superscript

$+$	=	nondimensionalization with friction velocity and wall units (ν/v^*)

Received 11 November 2004; revision received 23 March 2005; accepted for publication 4 April 2005.

*Lecturer, School of Engineering and Design.
†Professor of Mechanical Engineering, Fluid Dynamics Research Center. Senior Member AIAA.
‡Senior Lecturer, School of Mathematics.

I. Introduction

THE development of microelectromechanical systems (MEMS) has made the active control of turbulence a possibility. For turbulent boundary layers, vast arrays of MEMS sensors and actuators could, in principle, detect and modify the streaklike structures observed in the viscous sublayer.[1–3] These streaks are thought to be critical to the generation of turbulence,[4,5] and consequently, if they can be controlled, then so can the turbulence itself. Of many possible benefits, control of turbulence over a wing's surface could be used to reduce skin-friction drag or conversely to increase the turbulence level and thereby delay boundary-layer separation.

Several actuator designs have been considered for this application, with the microjet design shown in Fig. 1 being a popular proposal.[6] This device consists of a diaphragm, mounted within a plenum chamber, that is driven by a piezodevice attached to its underside. The diaphragm's motion produces pressure fluctuations inside the chamber that force fluid through an orifice in the lid. Originally, these devices were intended to operate in an oscillatory mode and create a massless or synthetic jet.[7–9] For practical

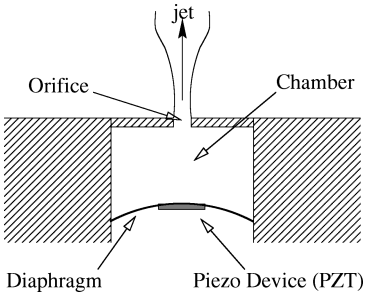

Fig. 1 Schematic of a microjet actuator. Design proposed by Coe et al.[6]

reasons, including the desire to avoid a strong influx into the system (for fear of ingesting dust), it has been suggested that an alternative mode of forcing is more appropriate for the turbulence-control application.[10,11] This consists of generating a sudden pressure rise in the plenum that, in turn, produces a "puff-like" jet from the orifice. The diaphragm is then slowly relaxed to its initial state.

Currently, little is known about how jet devices of this kind will affect the coherent structures of the turbulent boundary layer. Reliable experimental data in this area are limited, owing to the difficulty in constructing experiments that achieve dynamic similarity to MEMS-scale actuation in high-speed boundary layers. Also, direct numerical simulation of the turbulence and actuator (such as that performed by Carlson and Lumley[12]) is too computationally expensive for detailed studies to be performed at the Reynolds numbers of practical aeronautical interest.

In this paper, we describe the development of an economical numerical method for modeling the interaction between the turbulent streak and the microactuator. We use this tool to explore the basic concepts and viability of streak control by MEMS actuation.

II. Computational Model and Methods

There are three components to the actuator/streak modeling problem: the actuator, the boundary layer, and the streak. Here we consider each in turn.

The methods we have adopted to model the microjet actuator (Fig. 1) are given in some detail in Ref. 11. The diaphragm is modeled using thin-plate theory, with the dynamics and stiffness of the attached piezoceramic driver incorporated. For numerical economy, the fluid motion within the plenum chamber is not modeled, and instead the pressure is calculated using the perfect-gas law. Within the orifice, where viscous forces are more dominant, the one-dimensional Navier–Stokes equations are solved.

For calculating the boundary-layer disturbances generated by the microjet actuator, a novel form of the velocity-vorticity method has been adopted.[10,13] This has all of the advantages of conventional velocity-vorticity methods (notably, the absence of pressure from the governing equations), but has only three dependent variables rather than the usual six, which reduces the computational expense. Another important advantage compared with previous velocity-vorticity methods is that it replaces the nonrigorous, and strictly invalid, boundary conditions on vorticity at the wall with rigorously derived integral conditions (see in the following) that link the vorticity field with the boundary conditions imposed at the wall on the velocity field. This method has been fully validated over a wide range of established results in flow stability and other topics.[10,13–16]

The governing equations and numerical methods are almost identical to those described in our previous paper[10] on a related topic. The same reference quantities are used to nondimensionalize the governing equations, namely, the freestream flow speed U_∞, the boundary-layer displacement thickness δ^*, and kinematic viscosity ν. The coordinate system (x, y, z) corresponds respectively to the streamwise, spanwise, and wall-normal directions. The domain is semi-infinite such that $z = 0$ defines the lower boundary representing the solid surface plus any jet-type actuators. An actuator is represented by a distribution of unsteady wall-normal flow velocity over part of the surface $z = 0$.

We assume that there is a specified, undisturbed flow, represented by the dimensionless velocity $\bar{\boldsymbol{U}} = (U, 0, 0)$ and vorticity $\bar{\boldsymbol{\Omega}} = (0, \Omega_y, 0)$, where U and Ω_y correspond to the mean turbulent profiles. The total dimensionless velocity and vorticity fields are then decomposed into $\boldsymbol{U} = \bar{\boldsymbol{U}} + \boldsymbol{u}$ and $\boldsymbol{\Omega} = \bar{\boldsymbol{\Omega}} + \boldsymbol{\omega}$, where $\boldsymbol{u} = (u, v, w)$ and $\boldsymbol{\omega} = (\omega_x, \omega_y, \omega_x)$ represent perturbations from the prescribed mean flow.

We shall consider the governing equations for the perturbation flow variables only. These are divided into two sets. Namely, the primary variables $\{\omega_x, \omega_y, w\}$ and the secondary variables $\{\omega_z, u, v\}$. The secondary variables can be defined explicitly in terms of the former, and thus, in principle, eliminated from consideration. It can be shown[13] that the evolution of the three primary variables is governed by the following three equations only:

$$\frac{\partial \omega_x}{\partial t} + \frac{\partial N_z}{\partial y} - \frac{\partial N_y}{\partial z} = \frac{1}{Re}\nabla^2 \omega_x - \frac{\partial F_y}{\partial z} \tag{1}$$

$$\frac{\partial \omega_y}{\partial t} + \frac{\partial N_x}{\partial y} - \frac{\partial N_z}{\partial z} = \frac{1}{Re}\nabla^2 \omega_y \tag{2}$$

$$\nabla^2 w = \frac{\partial \omega_x}{\partial y} - \frac{\partial \omega_y}{\partial x} \tag{3}$$

where $\boldsymbol{N} = \bar{\boldsymbol{\Omega}} \times \bar{\boldsymbol{U}} + \boldsymbol{\omega} \times \bar{\boldsymbol{U}} + \boldsymbol{N}'$, $\boldsymbol{N}' = \boldsymbol{\omega} \times \boldsymbol{u}$, and $Re = U_\infty \delta^*/\nu$. The last term on the right-hand side of Eq. (1) represents the gradient of a fictitious body force; it acts as a vorticity source and will be explained in more detail in the following.

Because we are only interested in the fundamental coherent structures of the turbulent boundary layer (the streaks), we have adopted an undisturbed base flow corresponding to a time-averaged turbulent profile, with the aim of investigating linear perturbations from this. Thus for the simulations presented in the present paper, the governing equations are linearized by setting $\boldsymbol{N}' \equiv 0$. Strictly, then, our present approach is only valid provided the perturbations are of small amplitude. There is, however, considerable evidence to suggest that the development of the streaks is governed by a linear mechanism,[17–21] and moreover, their control can be modeled by a linear process,[22] so that this linear approach is justified, even though developed turbulence is characteristically nonlinear.

The base flow we have adopted is based on the velocity profile given in inverse analytical form by Spalding.[23] Because there is no corresponding analytical form for the mean wall-normal velocity and no straightforward way of obtaining one, the use of Spalding's approximate analytical velocity profile obliges us to assume a boundary layer of constant thickness in zero streamwise pressure gradient. This, perhaps, has some advantage because it has the merits of simplicity and of separating out the other effects from those of boundary-layer growth. In fact, for typical simulations the change in boundary-layer displacement thickness is very small. For example, if $Re = 5 \times 10^3$ and the streamwise extent of interest for studying actuation is 1000 wall units, using standard semi-empirical methods one can estimate that the displacement thickness would increase by about 1.25% over this distance.

The wall boundary conditions take the form

$$u(x, y, 0, t) = 0 \tag{4}$$

$$v(x, y, 0, t) = 0 \tag{5}$$

$$w(x, y, 0, t) = f(x, y, t) \tag{6}$$

where $f = 0$ except at an actuator exit where it equals the instantaneous jet velocity profile, which is either prescribed or given by the actuator model.

The definition of vorticity with use of conditions (4) and (5) gives[13] the integral conditions

$$\int_0^\infty \omega_y \, \mathrm{d}z = -\int_0^\infty \frac{\partial w}{\partial x} \, \mathrm{d}z \tag{7}$$

$$\int_0^\infty \omega_x \, \mathrm{d}z = \int_0^\infty \frac{\partial w}{\partial y} \, \mathrm{d}z \tag{8}$$

that are fully equivalent to the boundary conditions (4) and (5). They can therefore be viewed as constraints on the evolution of the primary variables ω_y and ω_x, respectively.

The inflow boundary conditions take the form of undisturbed flow so that $\omega_x = \omega_y = w = 0$ there. The computational domains used in our simulations extended sufficiently far in the streamwise direction that the flow perturbations were negligible at the downstream outflow boundary.

The sole difference from our previous formulation[10] is that a source term is added to the right-hand side of Eq. (1) for the streamwise vorticity perturbation ω_x. This source term takes the form of $\nabla \times \boldsymbol{F}$, where $\boldsymbol{F} = (0, F_y, 0)$ is a fictitious body force; thus, the source term can be written as

$$-\frac{\partial F_y}{\partial z} = -G \exp\left[-a(x - x_f)^2 - b(z - z_f)^2\right] \cos\, \beta y \qquad (9)$$

where G is the source strength; (x_f, z_f) denote the location of the source; and a and b are parameters specifying the width of the Gaussian function. The exponential term in Eq. (1) is a numerical approximation to the double delta function, $\delta(x - x_f)\delta(z - z_f)$. The form (9) used for the vorticity source will be further discussed and justified in Sec. III.

The computational domain is semi-infinite, stretching from a uniform wall at $z = 0$ to infinity in a direction normal to it, and is periodic in the spanwise direction. The governing equations are discretized using a centred finite difference scheme in the streamwise direction x and by a series of Chebyshev polynomials in the direction normal to the wall z. The discretization in the spanwise direction y is in the form of a Fourier-series expansion. The wall boundary conditions are implemented in exactly the same way as in Ref. 10.

At each time step for which the actuator is required to be active, the actuator model uses the pressure distribution over the orifice (calculated by the boundary-layer code) as input for calculating the microjet velocity. This is then incorporated into the boundary-layer simulation as a vertical velocity distribution at $z = 0$.

III. Streak Modeling

To simulate the effect of actuation on the sublayer streaks, it is necessary to generate model streaks relatively simply. This is done by activating the vorticity source, given in Eq. (9). It is probably helpful to explain first how such a source can be used as an approximate model of freestream turbulence for a study of the role of Klebanoff modes in laminar-turbulent transition.[24,25] When such a source is located in a uniform flow, the vorticity transport equation can be readily solved to show that it generates a narrow sheet of streamwise vorticity with a Gaussian profile in the z direction and with strength that varies sinusoidally in the spanwise direction.[26] Such a vorticity source generates a series of positive (high-speed) and negative (low-speed) streaks similar to those shown in Fig. 2. These flow structures are almost completely free of streamwise vorticity.[25] When the vorticity source is kept constant with time indefinitely, the streak-like flow structures will grow in strength until a steady-state value is reached. If the source is switched off after a period of time, the streaks will at first continue to grow in strength but will ultimately decay.[26] Very low-frequency sources of the form (9) will also generate Klebanoff-type modes.[25] The laminar boundary layer is found to be unreceptive to steady and low-frequency spanwise vorticity sources of the form (9), although oscillating sources of the appropriate frequency will generate Tollmien–Schlichting waves.

When the vorticity source is immersed in a turbulent boundary layer, the sheet of streamwise vorticity it generates acts as an approximate model for the vortex structures (hairpin vortices) found in the transitional and log-law regions of the turbulent boundary layer. The idea of using a fictitious body force as a vorticity source came to us from Meitz[27] and Fasel.[25] However, in their method it is the body force itself that is proportional to $\delta(x - x_f)\delta(z - z_f)$, implying that the vorticity source is proportional to the derivative of a double delta function. This makes a less suitable simple model of the sort of streamwise vortex structures found in a turbulent boundary layer.

When the vorticity source is activated, streak-like structures begin to grow in the sublayer with much the same characteristics as just described for the Klebanoff modes in a laminar boundary layer. Because we are running our numerical code with the nonlinear terms suppressed, it cannot model the nonlinear aspects of the streak cycle,

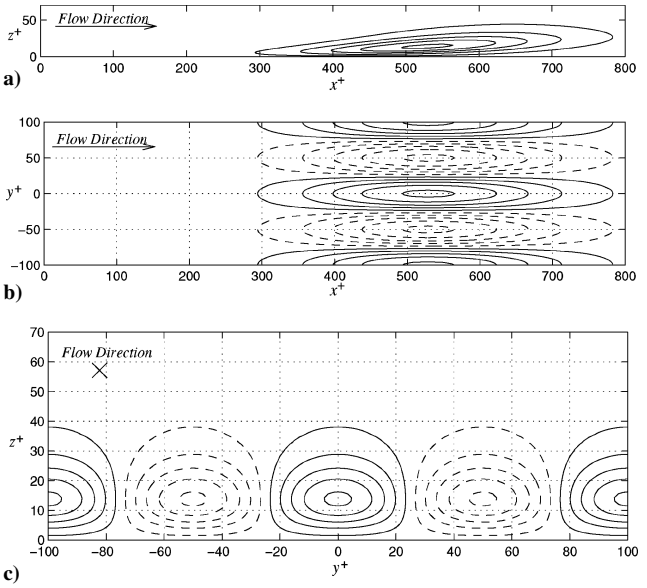

Fig. 2 Optimum streak at its maximum amplitude. Side-, plan-, and front-view contours of streamwise velocity perturbation at $t^+ = 50$. The nth contour is at $u^+ = \pm[0.019 + 0.038\,(n - 1)]$, where —— and – – – denote positive and negative values, respectively: a) side view at $y^+ = 0$; b) plan view taken at the wall-normal position having the greatest velocity for each streamwise position; and c) front view at $x^+ = 528$, where $Re \approx 5 \times 10^3$. Numerical parameters are $\Delta x^+ = 20.4$, $\Delta t^+ = 0.4$, $N_c = 64$, and $N_f = 1$.

such as bursting. Nor can our model sensibly be used to shed much light on the long-running debates on the role of the outer part of the boundary layer or whether it is the streaks or the "hair-pin vortices" that are the primary structures. It is, perhaps, worth noting that the hairpin vortices appear to be fairly universal structures of turbulent flow. Not only have they been found by many authors in turbulent boundary layers and other wall shear layers,[28] but Rogers and Moin[29] found them in a direct numerical simulation of homogeneous turbulence. However, it was only when the homogeneous turbulence was subjected to high shear rate that streaks were generated similar to those found in turbulent channel flows with the same shear-rate parameter.[30] This suggests all that is needed to generate streaks are the appropriate vortical structures and a sufficiently high shear rate. Our model is not in conflict with this view. It shows that the streaks are a response by the sublayer to forcing by streamwise vorticity with a particular optimized spanwise length scale. As the streaks grow, they generate inflexion points locally in the velocity profile. These inflexion points could well play a crucial role in the subsequent nonlinear development of the streaks, as suggested by many previous authors.[28]

Despite its evident limitations, we argue that our linear Klebanoff-mode model for the sublayer streaks is reasonably adequate for studying control. We can make an analogy with the classic route to transition whereby small-amplitude Tollmien–Schlicting waves grow exponentially, as described by linear hydrodynamic stability theory, until sufficiently large for nonlinear effects to take over and for transition proper to ensue. In this case, if the growth of Tollmien–Schlichting waves is reduced or suppressed in their linear growth phase, transition proper will be delayed or suppressed entirely. Likewise in our proposed scenario for the sublayer streaks, if their growth rate is reduced/increased in the initial linear phase, the bursting frequency will be reduced/increased with consequent reduction/augmentation of the turbulent shear stress. Incidentally, the fact that alternating high- and low-speed streaks are generated means that for linear simulations the spanwise-averaged velocity perturbation is zero. This provides some further justification for the use of the mean turbulent velocity profile as our undisturbed base flow.

The ideas behind our approximate model for the sublayer streaks are not, of course, entirely new. It is known that three-dimensional disturbances in a shear flow can grow algebraically, termed as such

to distinguish it from exponential growth. This was demonstrated by Ellingson and Palm[31] and Landahl[17] for three-dimensional perturbations in an inviscid shear flow. The inviscid algebraic growth, together with a viscous-induced damping, constitutes what is sometimes called transient growth. This phenomenon has been demonstrated in viscous shear flows by Hultgren and Gustavsson,[32] Butler and Farrell,[33] and Henningson et al.[34] Transient or algebraic growth is believed to be the cause of "bypass" transition in boundary layers. It is thought that small perturbations might grow sufficiently during the transient growth period for nonlinear effects or secondary instabilities to induce transition, hence bypassing traditional mechanisms. The Klebanoff mode,[24,25,35–38] generated by freestream turbulence, is generally thought to be a manifestation of algebraic/transient growth.[39–41] This hypothesis is consistent with the findings of Landahl,[17,18] Breuer and Haritonidis,[42] and Henningson et al.,[34] who have demonstrated how the "lift-up" effect (a phrase introduced by Kline et al.[5] and subsequently used by Landahl to describe the mechanism of algebraic growth) leads to longitudinal streaky structures similar to those observed in the Klebanoff mode.

Landahl[17,18] and Butler and Farrell[33] made a connection between the longitudinal streaks in a fully turbulent boundary layer and algebraic growth. There is, therefore, an implied equivalence between the Klebanoff mode in the transitional boundary layer and the streamwise sublayer streaks in a fully turbulent boundary layer. The algebraic-growth mechanism induces streaks in both cases; it is forced by freestream turbulence in the transitional case and for a turbulent boundary layer by the streamwise vortical structures in log-law and transitional regions. This furthers the analogy between the transitional and the turbulent boundary layer.[43]

Initially, by way of verification, we ran our boundary-layer code with the Blasius laminar velocity as the undisturbed base flow and the vorticity source located just above the boundary-layer edge. Figure 3 shows the results of a series of such simulations that show how the relative magnitude of streaks generated by vorticity sources with fixed strength G varies with spanwise wave number β. The wave number that appears to be most receptive to streak generation is very close to the dominant spanwise mode observed by Klebanoff[24] in his work on boundary-layer transition (value reported in Herbert and Lin[39] and Bertolotti[40]). Given the apparent similarity between the Klebanoff mode and the streaks in a turbulent boundary layer, it seems reasonable to use similar methods for their modeling. And so, here we have used the vorticity source given in Eq. (9) to find the dominant mode of streak development within the turbulent mean-velocity profile. There are, however, two main differences from the Klebanoff-mode modeling. First, an optimum normal position for the body force is sought, whereas in the Klebanoff case, freestream forcing is used at a fixed distance from the wall. Second, the body forcing acts for a discrete time rather than continuously. This time has been chosen to match the nondimensional period ($t^+ = 15$) of suction used by Gad-el-Hak and Hussain[44] to artificially generate streaks.

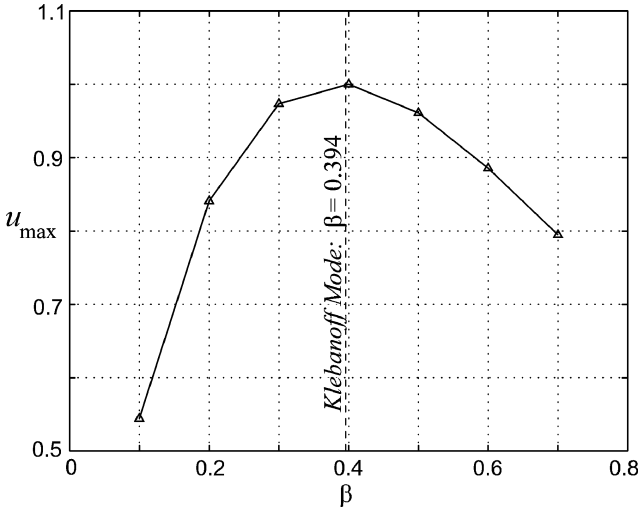

Fig. 3 Maximum streak magnitude u_{max} vs the spanwise wave number of the applied body force β. The vertical dashed line is from the Klebanoff experiments as reported in Herbert and Lin[39] and Bertolotti,[40] $Re \approx 1720.7$.

Our method is somewhat similar to that of Butler and Farrell[45] who sought an optimum perturbation to a turbulent mean-velocity profile. They achieved some success by defining the optimum as corresponding to the largest growth in disturbance kinetic energy during a particular period. The choice of this period was the turbulent eddy turnover time ($t^+ \approx 100$). Kim and Lim[22] suggested that this approximation was incorrect, and that the time for optimum growth is, in fact, much shorter. Here, the optimum streak is not restricted to growth during a predetermined period, but is defined as the streak with the largest streamwise velocity at any time during its evolution (in fact, we find the optimum streak reaches its maximum at around $t^+ = 50$, which is significantly shorter than the eddy turnover time and therefore in agreement with Kim and Lim[22]). Our model for the sublayer streak also bears some resemblance to the recent work of Baig and Chernyshenko.[46] They generate the streaks with a random velocity field in a direct numerical simulation of quasi-two-dimensional, decaying turbulent channel flow. Our simplified linear model appears to be compatible with their nonlinear one.

The near-wall region of the turbulent boundary layer is characterized by the friction velocity v^* and the wall unit ν/v^*. For the simulations in this paper, we have chosen $v^* = 10$ m/s and $\nu/v^* = 1.5$ μm. Based on Spalding's analytical velocity profile,[23] these values correspond to $\delta^* \approx 0.3$ mm and $U_\infty \approx 250$ m/s.

Figure 4 shows the maximum streamwise velocity perturbation (streak magnitude) plotted against the spanwise wave number of the applied body force. A clear optimum appears at around 100 wall units (100 ν/v^*), which is in agreement with the average streak spacing observed in many experimental studies, including those of Kline et al.[5] In fact, using the same model for the sublayer streaks, Ali[47] has reproduced the gradual increase in average streak spacing with a rise in Reynolds number seen in experiments. His results for a turbulent boundary layer over a compliant wall also agree well with the experimental data of Lee et al.[48] showing the increase in the spanwise streak spacing caused by wall compliance. For all of these results, including those of Figs. 2, 4, and 5, the position of the body force in the wall-normal direction has been chosen to optimize the streak magnitude for each spanwise wave number considered. The optimum value was found to be $z_f^+ \simeq 18$, suggesting that it is the legs of the hairpin vortices that descend well into the transitional layer that generate the strongest streaks. The spatial and temporal development of the optimum streak is shown in Fig. 5 and side-, plan-, and front-view contours of the streak (at $t^+ = 50$) are shown in Fig. 2. The positive and negative velocity perturbations correspond to high- and low-speed streaks, respectively. The streaks do continue to elongate after $t^+ = 50$, although the magnitude of the streamwise velocity reduces. At the later times shown in Fig. 5, the streamwise convection velocity of the streak is approximately $11v^*$. This is in close agreement with the experimental observations of Johansson et al.,[49] corresponding to $13v^*$, and the numerical results

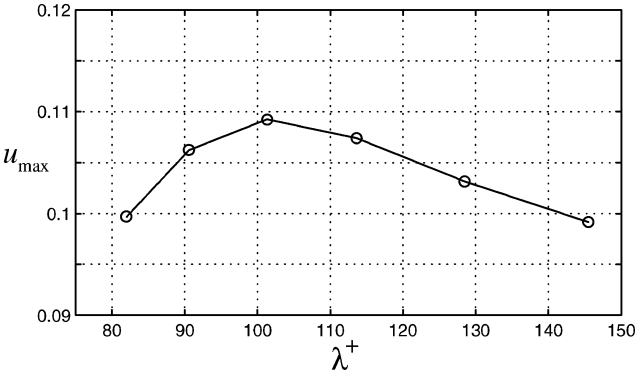

Fig. 4 Maximum streak magnitude u_{max} vs the spanwise wavelength of the applied body force λ^+: $Re \approx 5 \times 10^3$.

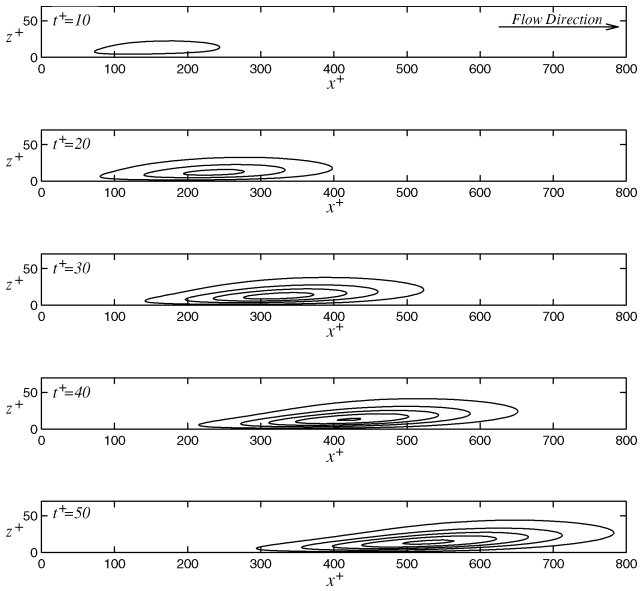

Fig. 5 Temporal and spatial development of the optimum streak. Side-view contours of streamwise velocity perturbation at times leading to the point of the streak's maximum magnitude. The *n*th contour is at $u^+ = 0.019 + 0.038\,(n-1)$. The body force is positioned at $x^+ = 125$, $z^+ = 18.4$, and is applied from $t^+ = 0$ to 15: $Re \approx 5 \times 10^3$. Numerical parameters are $\Delta x^+ = 20.4$, $\Delta t^+ = 0.4$, $N_c = 64$, and $N_f = 1$.

of Johansson et al.,[49] corresponding to $10.6v^*$. This numerical and experimental validation gives us confidence that we have developed a satisfactory model for the sublayer streaks (during the early stages of their development).

In the real turbulent boundary layer the streaks are much more randomized than Fig. 2 would suggest. What is depicted here could be thought of as cleaned-up streaks. These represent the strongest streaks generated by the optimum streamwise vortical structures. In the real turbulent boundary layer there is a wide range of streamwise vortical structures generating streaks of various strengths and spanwise spacing. In some respects, we can again draw an analogy with Tollmien–Schlichting waves. Our streaks are analogous to the clean monochromatic waves created by a vibrating ribbon. The fastest growing such waves are certainly seen in natural transition, but they are masked to some extent by the presence of other frequencies.

IV. Streak-Control Simulations

The streaks modeled in the preceding section are used here to test the effectiveness of MEMS actuation in targeted control. There are two basic concepts to be investigated: streak intensification and streak suppression. The motive of streak intensification is to increase the bursting frequency and thereby promote turbulence production. This is achieved by making the structure more prone to the spanwise inflectional instability[50] or to the onset of nonlinear effects. Either way, this means increasing the growth of the streaks. The motive of streak suppression is to reduce the bursting frequency, thereby inhibiting the production of turbulence and reducing the wall shear stress. This is achieved by reducing the growth of the streaks.

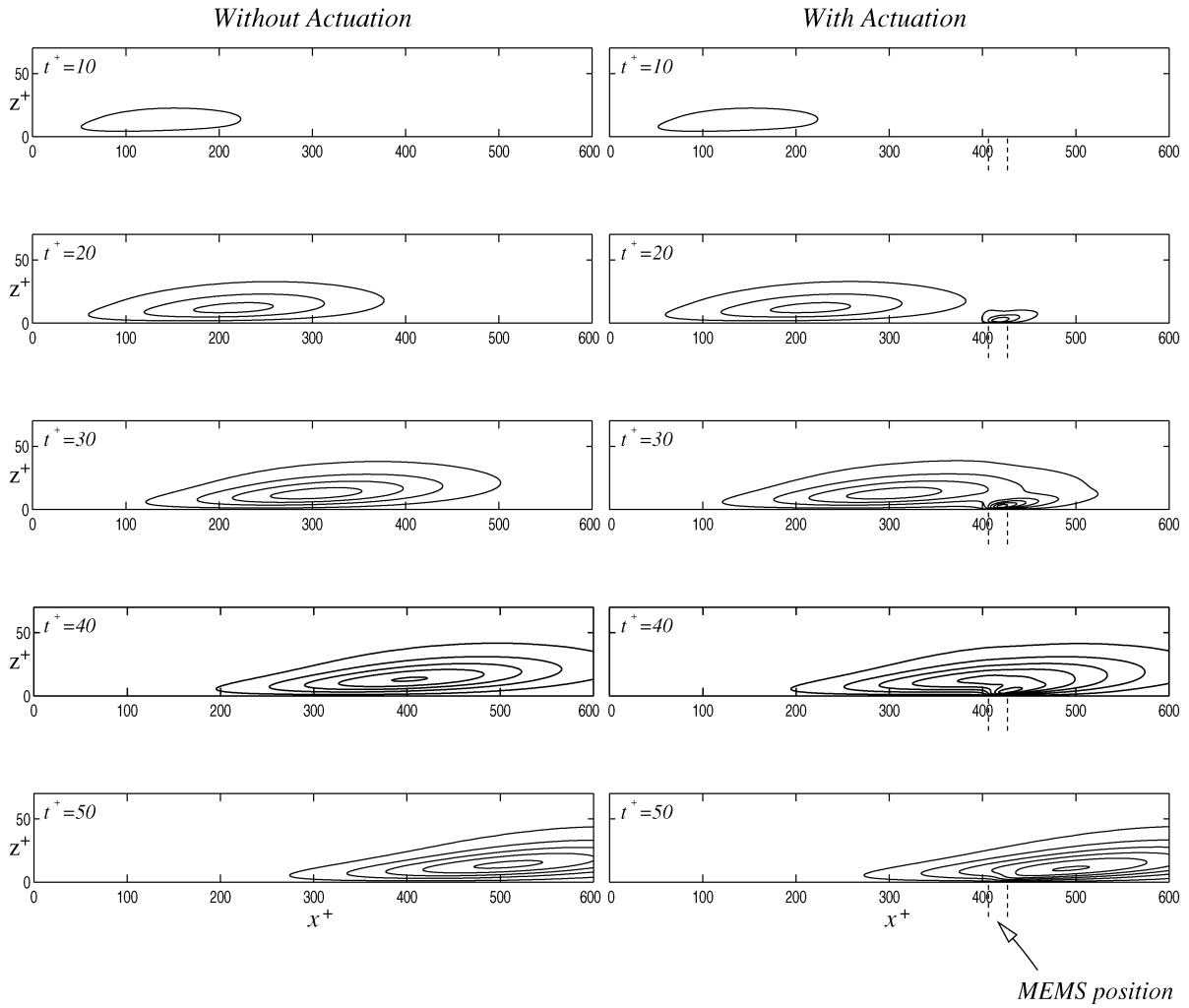

Fig. 6 Effect of actuation on the development of a low-speed streak. The actuation occurs during the period $t^+ = 10$–50, and its location is indicated by the vertical dashed line at $x^+ = 407$–427 ($r = 15$ μm, $t_p = 6$ μs, $V_m = 2.56$ m s^{-1}). The *n*th contour indicates a velocity perturbation of $u^+ = -[0.019 + 0.038\,(n-1)]$, where the solid line denotes negative values. This simulation is also equivalent to negative actuation (suction) on a high-speed streak; in this case contour values would be inverted, where $Re \approx 5 \times 10^3$. Numerical parameters are $\Delta x^+ = 3.33$, $\Delta t^+ = 0.0645$, $N_c = 32$, and $N_f = 16$.

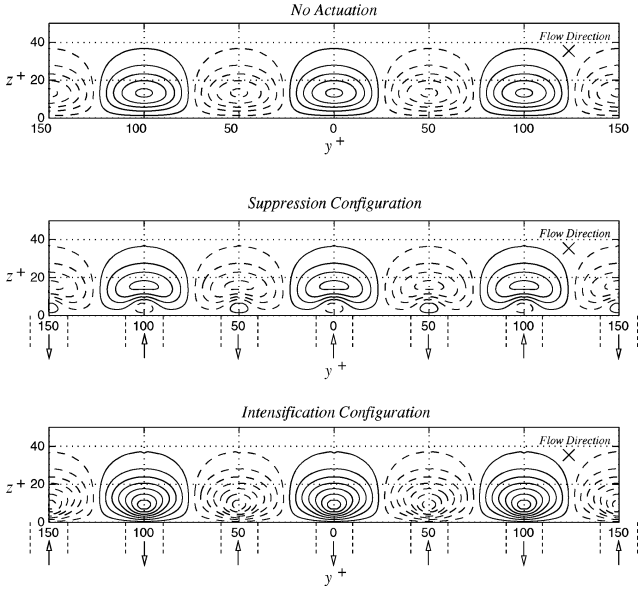

Fig. 7 Effect of a spanwise distribution of actuators on an array of high- and low-speed streaks. Front-view contours of streamwise velocity perturbation at $t^+ = 50$ and $x^+ = 528$; the nth contour is at $u^+ = \pm[0.019 + 0.038\,(n-1)]$, where —— and – – – denote positive and negative values, respectively: a) no actuation $V_m = 0$; b) suppression configuration-suction under low-speed streaks and blowing under high-speed streaks, $V_m = \pm 5.06$ m s^{-1}; and c) intensification configuration-suction under high-speed streaks and blowing under low-speed streaks, $V_m = \pm 5.06$ m s^{-1}. The spanwise positions of the MEMS are indicated by the vertical dashed line at $y^+ = 50i - 10$ and $50i + 10$, for $i = -3, -2, \ldots, 3$ (for each, $r = 15$ μm and $t_p = 6$ μs), where $Re \approx 5 \times 10^3$. Numerical parameters are $\Delta x^+ = 3.33$, $\Delta t^+ = 0.0645$, $N_c = 32$, and $N_f = 16$.

A. Prescribed Simulations

In this section the actuator is incorporated into the boundary-layer code as a prescribed boundary condition, that is, the actuator model is not used. The velocity profile at the exit of the orifice is assumed to be parabolic with a centerline velocity V_c, which varies in time as follows:

$$V_c = V_m \sin(t\pi/t_p) \qquad \text{for} \qquad 0 \le t \le t_p$$
$$V_c = 0 \qquad \text{for} \qquad t > t_p \tag{10}$$

Prescribing the velocity boundary condition in this manner allows a large number of simulations to be performed at relatively low computational cost.

Figure 6 shows the successful intensification of a low-speed streak using microjet actuation. The upward velocity introduced by the microjet moves low-speed fluid away from the wall and into a higher-speed region of the boundary layer. This generates a negative streamwise velocity perturbation, which serves to intensify the low-speed streak overhead. The simulations shown in this paper are linear and can therefore be made equivalent to those of opposite sign. For example, in this case the results can be inverted to represent the effect of suction on a high-speed streak.

Figure 7 is a front view of a spanwise array of actuators in both suppression and intensification configurations. This implements the concept suggested in Fig. 1a of Gad-el-Hak and Blackwelder.[51] We have found that for streak intensification a positive actuation (blowing) should be applied to low-speed streaks and negative actuation (suction) to high-speed streaks. The opposite is true for streak suppression.

The maximum jet velocities for Figs. 6 and 7 are of the order of 1 or 2% of the freestream flow speed, and so these are very weak jets. As the simulations are linear, any reduction (or intensification) of the streak velocity perturbation as a result of the control should scale proportionally with an increase in jet velocity magnitude.

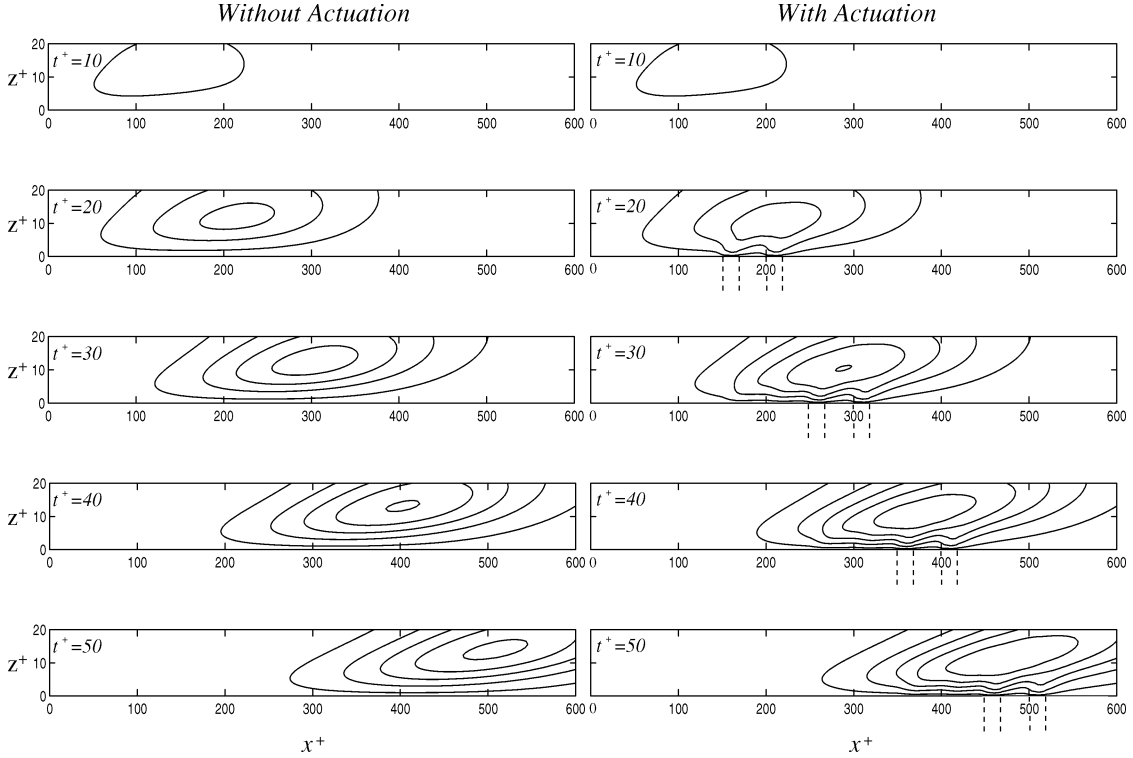

Fig. 8 Effect of a streamwise distribution of weak microjets on the development of a low-speed streak. Side-view contours ($y^+ = 0$) of streamwise velocity perturbation at times leading to the point of the streak's maximum magnitude; the nth contour is at $u^+ = -[0.019 + 0.038\,(n-1)]$, where the solid line denotes negative values. There are eight actuators in total, each with $r = 15$ μm, $t_p = 3$ μs, and $V_m = 0.63$ m s^{-1}. The mth actuator is positioned between $x^+ = 100 + 50m$ and $120 + 50m$ (indicated by the vertical dashed line), and its actuation period is from $t^+ = 5 + 5m$ to $25 + 5m$, for odd m, and from $t^+ = 5m$ to $20 + 5m$, for even m. This simulation is also equivalent to negative actuation (suction) on a high-speed streak; in this case contour values would be inverted, where $Re \approx 5 \times 10^3$. Numerical parameters are $\Delta x^+ = 3.33$, $\Delta t^+ = 0.0645$, $N_c = 32$, and $N_f = 16$.

There is a difficulty in using a lone actuator to control a rapidly convecting streak, and this is highlighted in Fig. 6. The actuator has to be triggered a significant period of time before the streak is in its immediate vicinity in order for the maximum jet velocity to occur when the streak is directly overhead. Necessarily, some of the actuator's output is wasted. As an alternative actuation strategy, here we propose the use of a streamwise distribution of weaker microjets, rather than a stronger lone actuator, which can be triggered when a streak is in their proximity. Figure 8 illustrates the effectiveness of such a strategy. (Note that the combined mass outflow of the distributed microjets is equal to that of the lone actuator used in Fig. 6.) Although the maximum streak intensification created by the microjet array does not surpass that of the lone actuator, the low-speed streak is intensified at *all* stages of its development, and approximately four times less energy is required.

B. A Coupled Simulation

Here we combine the numerical actuator and boundary-layer models to perform a coupled simulation. In these simulations the pressure of the boundary-layer affects the output of the microjet actuator and vice versa. Previous numerical studies have suggested that the interactive effect of the actuator and boundary layer can be significant.[10]

One of the benefits of performing the noncoupled prescribed simulations of the preceding section is that, because of the linearity of the model, the streaks and the jets can be calculated separately on different grids with different grid resolutions. When combining the two onto a mutual grid for a coupled simulation, the combination of the maximum grid spacing (determined by the scale of the microjet) and the minimum domain length (determined by the scale of the streak) dictates a very demanding computation.

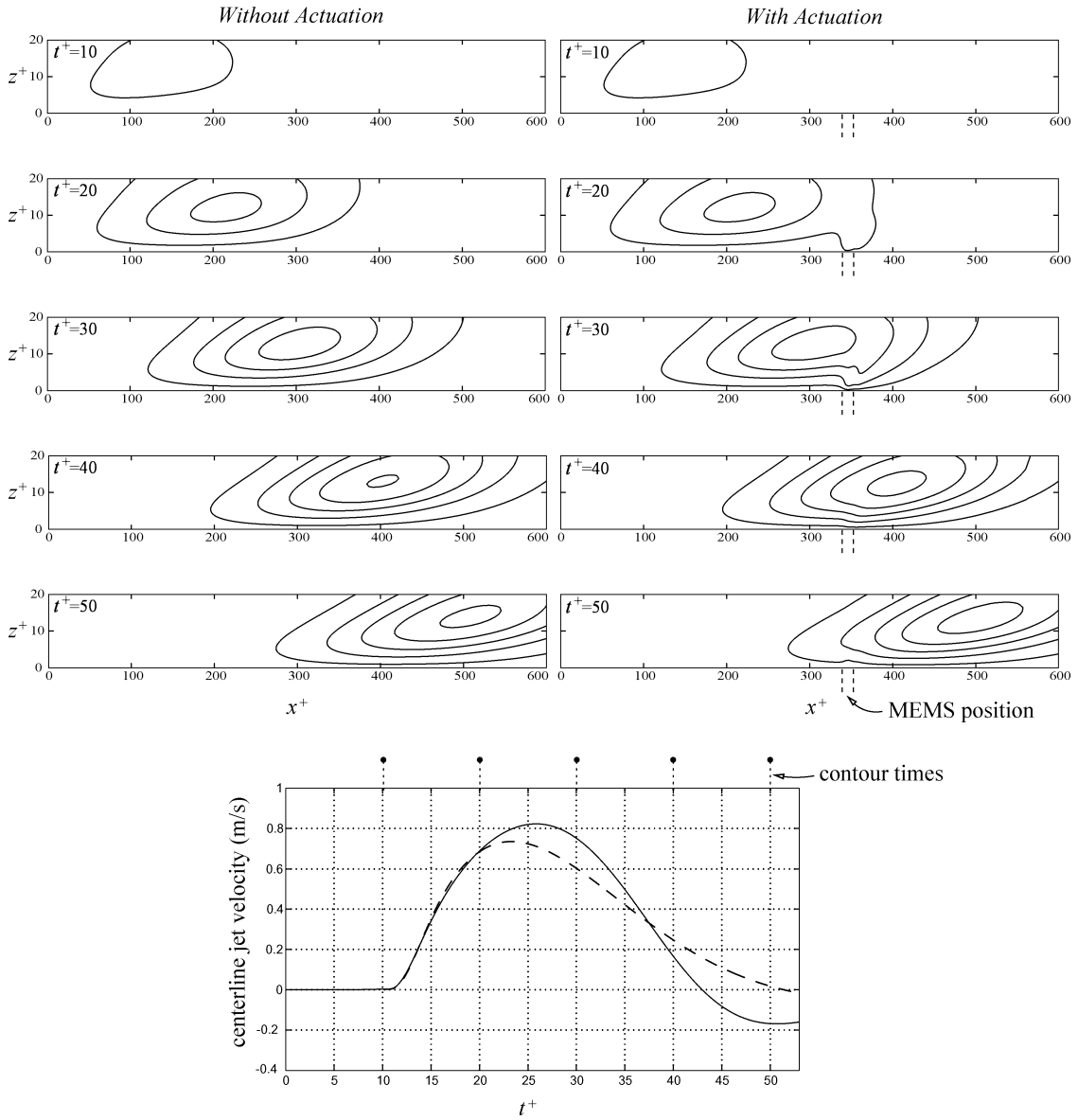

Fig. 9 Interaction of a microjet actuator and the development of a low-speed streak. Side-view contours ($y^+ = 0$) of streamwise velocity perturbation at times leading to the point of the streak's maximum magnitude; the nth contour is at $u^+ = -[0.019 + 0.038\,(n-1)]$, where the solid line denotes negative values. The MEMS location is indicated by the vertical dashed line at $x^+ = 340.13$–353.47 ($r = 10$ μm). For reference, the evolution of actuator jet velocity is shown beneath the contour plots; the solid line indicates the actual velocity, and the dashed line the velocity if the jet were issuing into an undisturbed boundary layer. This simulation is also equivalent to negative actuation on a high-speed streak; in this case contour values and the velocity plot would be inverted. $Re \approx 5 \times 10^3$. Actuator specification: diameter and length of exit orifice are 10 and 20 μm, respectively. Depth of plenum chamber is 250 μm. Diameter, thickness, elastic modulus, Poisson ratio, and density of diaphragm are 100 μm, 1 μm, 100 GPa, 0.27, and 2300 kg/m^3, respectively. Diameter, thickness, elastic modulus, Poisson ratio, and density of piezoceramic are 86 μm, 1.22 μm, 63 GPa, 0.3, and 7600 kg/m^3, respectively. The combined structural damping of the diaphragm and piezoceramic is 100 kN s/m^3. The voltage drop across the piezoceramic is 800 kV/m, and the piezoelectric constant is 220×10^{-12} m/V.

However, with some reasonable assumptions this problem can be circumvented.

As the streak is much larger than the actuator, it can be safely assumed that the pressure variations over the orifice caused by the streak disturbance do not need to be resolved at the same scale as the actuator's disturbance. If this is accepted, a coupled simulation can be performed in an undisturbed boundary layer (with a small domain) by superposing the pressure resulting from the streak (calculated earlier on a larger and coarser domain) onto the pressure disturbance caused by the actuator. The final result is then obtained by superposing both streak and streak/actuator results onto a common grid. Further details of this numerical method can be found in Ref. 52.

Figure 9 shows the result of a coupled simulation of streak control using microjet actuation. As in Fig. 6, the low-speed streak is enhanced by the downstream actuation of the microjet. However, the effect is less pronounced in this case because the microjet considered is smaller, weaker, and shorter than the prescribed-jet function. Even so, the simulation presented in Fig. 8 has shown that a streamwise array of relatively weak microjets can be used to provide very efficient control.

In the absence of a streak, the output velocity of the microjet considered in Fig. 9 is only slightly negative (inflowing) at later times (indicated in Fig. 9 by the dashed line in the velocity-time plot). However, in the fully coupled simulation the pressure footprint of the convecting streak contributes to produce a significant microjet inflow (indicated in Fig. 9 by the solid line in the velocity-time plot). It is easy to envision that more violent disturbances, such as streak bursting, could affect the output of microjets dramatically and even create actuation when the device is intended to be inactive. If this type of actuator can be affected by the nondeterministic pressure fluctuations of the turbulent boundary layer, this highlights a major flaw with the device—its inherent unpredictability. However, for these computations the voltage assumed to be supplied to the actuator is very low, approximately 1 V. This could be greatly increased in practice, which would increase the strength of the microjet and make it less susceptible to the influence of the pressure field.

V. Conclusions

We have described the application of economical numerical methods to the modeling of the interaction between sublayer streaks and microjet actuators. We have noted that in the literature there is an implied analogy between the Klebanoff mode and the turbulent streaks, and we have used this to guide our modeling. By seeking an optimum response of a turbulent mean-velocity profile to a streamwise vorticity source generated by an applied body force, we have found streaks with the same structural and dynamical characteristics as those observed experimentally and numerically. We are confident, then, that this provides a satisfactory model for simple analysis.

By performing a series of noncoupled simulations (with the actuation incorporated into the boundary-layer code as a prescribed boundary condition), we have established that microjets, in either blowing or suction mode, can be used to suppress or intensify either low-speed or high-speed streaks. However, because suction is problematic, for practical reasons only blowing can be considered. Given this restriction, low-speed streaks should be targeted for separation delay (as this would intensify the bursting process and lead to high turbulence levels) and high-speed streaks targeted for skin-friction reduction (as this would inhibit the bursting process).

A fully coupled simulation of the interaction between the microjet and the streak has been presented. Although the impact of the single microjet is only slight, we have demonstrated with noncoupled simulations how a streamwise array of weak jets might be used to control streaks effectively.

The coupled simulation raises a point of considerable concern, and this is that weak microjet actuators can be significantly affected by pressure variations within the boundary layer. Real turbulence is nondeterministic, and this suggests that the microjet can behave erratically in its working environment. The assumed voltage supply to the actuators is at a very low level; increasing the voltage would produce stronger jets, and so it is entirely possible that undue influence of the background pressure field could be eliminated in this way. However, the study of the interaction of strong control jets with the streak structures is probably beyond the scope of our linearized model.

Acknowledgments

The research presented here was undertaken as part of the AEROMEMS project (an investigation into the viability of microelectromechanical systems technology for boundary-layer control on aircraft), which was a collaboration between British Aerospace; Dassault Aviation; Centre National de la Recherche Scientifique; and the Universities of Warwick, Manchester, Berlin, Madrid, Athens, Lausanne, and Tel-Aviv. The project was managed by British Aerospace and was partially funded by the CEC under the IMT initiative (Project Ref: BRPR CT97-0573).

References

[1]Gad-el-Hak, M., "Interactive Control of Turbulent Boundary Layers: A Futuristic Overview," *AIAA Journal*, Vol. 32, No. 9, 1994, pp. 1753–1765.

[2]Gad-el-Hak, M., "Modern Developments in Flow Control," *Applied Mechanics Reviews*, Vol. 49, No. 8, 1996, pp. 365–379.

[3]Gad-el-Hak, M., *Flow Control: Passive, Active, and Reactive Flow Management*, Cambridge Univ. Press, London, 2000.

[4]Blackwelder, R. F., and Eckelmann, H., "Streamwise Vortices Associated with the Bursting Phenomenon," *Journal of Fluid Mechanics*, Vol. 94, 1979, pp. 577–594.

[5]Kline, S. J., Reynolds, W. C., Schraub, F. A., and Runstadler, P. W., "The Structure of Turbulent Boundary Layers," *Journal of Fluid Mechanics*, Vol. 30, 1967, pp. 741–773.

[6]Coe, D. J., Allen, M. G., Trautman, M. A., and Glezer, A., "Micromachined Jets for Manipulation of Macro Flows," Solid-State Sensor and Actuator Workshop, June 1994, pp. 243–247.

[7]Hassan, A. A., and JanakiRam, R. D., "Effects of Zero-Mass 'Synthetic' Jets on the Aerodynamics of the NACA-0012 Airfoil," *Journal of the American Helicopter Society*, Vol. 43, No. 4, 1998, pp. 303–311.

[8]Smith, D. R., Amitay, M., Kibens, V., Parekh, D., and Glezer, A., "Modification of Lifting Body Aerodynamics Using Synthetic Jet Actuators," AIAA Paper 98-0209, 1998.

[9]Crook, A., Sadri, A. M., and Wood, N. J., "The Development and Implementation of Synthetic Jets for the Control of Separated Flow," AIAA Paper 99-3176, 1999.

[10]Lockerby, D. A., Carpenter, P. W., and Davies, C., "Numerical Simulation of the Interaction of Microactuators and Boundary Layers," *AIAA Journal*, Vol. 36, No. 1, 2002, pp. 67–73.

[11]Lockerby, D. A., and Carpenter, P. W., "Modeling and Design of Microjet Actuators," *AIAA Journal*, Vol. 42, No. 2, 2004, pp. 220–227.

[12]Carlson, H. A., and Lumley, J. L., "Active Control in the Turbulent Wall Layer of a Minimal Flow Unit," *Journal of Fluid Mechanics*, Vol. 329, 1996, pp. 341–371.

[13]Davies, C., and Carpenter, P. W., "A Novel Velocity-Vorticity Formulation of the Navier–Stokes Equations with Application to Boundary-Layer Disturbance Evolution," *Journal of Computational Physics*, Vol. 172, Dec. 2001, pp. 119–165.

[14]Davies, C., and Carpenter, P. W., "Global Behaviour Corresponding to the Absolute Instability of the Rotating-Disc Boundary Layer," *Journal of Fluid Mechanics*, Vol. 486, 2003, pp. 287–329.

[15]Bowles, R. I., Davies, C., and Smith, F. T., "On the Spiking Stages in Deep Transition and Unsteady Separation," *Journal of Engineering Mathematics*, Vol. 45, No. 1, 2003, pp. 227–245.

[16]Davies, C., "Numerical Simulation of Boundary-Layer Disturbance Evolution," *Philosophical Transactions of the Royal Society A: Mathematical, Physical and Engineering Sciences*, Vol. 363, No. 1830, 2005, pp. 1109–1118.

[17]Landahl, M. T., "A Note on Algebraic Instability of Inviscid Parallel Shear Flows," *Journal of Fluid Mechanics*, Vol. 98, 1980, pp. 243–251.

[18]Landahl, M. T., "On Sublayer Streaks," *Journal of Fluid Mechanics*, Vol. 212, 1990, pp. 593–614.

[19]Johansson, A. V., Alfredsson, P. H., and Eckelmann, H., *Advances in Turbulence*, Springer-Verlag, Berlin, 1987.

[20]Rathnasingham, R., and Breuer, K. S., "Coupled Fluid-Structural Characteristics of Actuators for Flow Control," *AIAA Journal*, Vol. 35, No. 5, 1997, pp. 832–837.

[21]Rathnasingham, R., and Breuer, K. S., "System Identification and Control of a Turbulent Boundary Layer," *Physics of Fluids*, Vol. 9, No. 7, 1997, pp. 1867–1869.

[22]Kim, J., and Lim, J., "A Linear Process in Wall-Bounded Turbulent Shear Flows," *Physics of Fluids*, Vol. 12, No. 8, 2000, pp. 1885–1889.

[23]Spalding, D. B., "A Single Formula for the Law of the Wall," *Journal of Applied Mechanics*, Vol. 28, 1961, pp. 455–457.

[24]Klebanoff, P., "Effects of Freestream Turbulence on a Laminar Boundary Layer," *Bulletin of the American Physical Society*, Vol. 10, No. 11, 1971, p. 1323.

[25]Fasel, H., "Numerical Investigation of the Interaction of the Klebanoff Mode with a Tollmien-Schlichting Wave," *Journal of Fluid Mechanics*, Vol. 172, 2002, pp. 1–33.

[26]Kudar, K., "Flow Control Using Pulsed Jets," Ph.D. Dissertation, School of Engineering, Univ. of Warwick, Coventry, England, Nov. 2004.

[27]Meitz, H. L., "Numerical Investigation of Suction in a Transitional Flat-Plate Boundary Layer," Ph.D. Dissertation, Univ. of Arizona, 1996.

[28]Panton, R., "Overview of the Self-Sustaining Mechanisms of Wall Turbulence," *Progress in the Aerospace Sciences*, Vol. 37, No. 4, 2001, pp. 341–383.

[29]Rogers, M., and Moin, P., "The Structure of the Vorticity Field in Homogeneous Turbulent Flows," *Journal of Fluid Mechanics*, Vol. 176, 1987, pp. 33–66.

[30]Lee, M., Kim, J., and Moin, P., "Structure of Turbulence at High Shear Rate," *Journal of Fluid Mechanics*, Vol. 216, 1990, pp. 561–583.

[31]Ellingson, T., and Palm, E., "Stability of Linear Flow," *Physics of Fluids*, Vol. 18, No. 4, 1975, pp. 487, 488.

[32]Hultgren, L. S., and Gustavsson, L. H., "Algebraic Growth of Disturbances in a Laminar Boundary Layer," *Physics of Fluids*, Vol. 24, No. 6, 1981, pp. 1000–1004.

[33]Butler, K. M., and Farrell, B. F., "Three-Dimensional Optimal Perturbations in Viscous Shear Flow," *Physics of Fluids*, Vol. 4, No. 8, 1992, pp. 1637–1650.

[34]Henningson, D. S., Lundbladh, A., and Johansson, A. V., "A Mechanism for By-Pass Transition from Localized Disturbances in Wall-Bounded Shear Flows," *Journal of Fluid Mechanics*, Vol. 250, 1993, pp. 169–207.

[35]Westin, K. J. A., Boiko, A. V., Klingmann, B. G. B., Kozlov, V. V., and Alfredsson, P. H., "Experiments in a Boundary Layer Subjected to Free Stream Disturbances," *Journal of Fluid Mechanics*, Vol. 281, 1994, pp. 193–245.

[36]Kendall, J. M., "Experimental Study of Disturbances Produced in a Pre-Transitional Laminar Boundary Layer by Weak Free Stream Turbulence," AIAA Paper 85-1695, 1985.

[37]Andersson, A., Berggren, M., and Henningson, D. S., "Optimal Disturbances and By-Pass Transition in Boundary Layers," *Physics of Fluids*, Vol. 11, No. 1, 1999, pp. 134–150.

[38]Leib, S. J., Wundrow, D. W., and Goldstein, M. E., "Effect of Free-Stream Turbulence and Other Vortical Disturbances on a Laminar Boundary-Layer," *Journal of Fluid Mechanics*, Vol. 380, 1999, pp. 169–203.

[39]Herbert, T., and Lin, N., "Studies on Boundary-Layer Receptivity with Parabolized Stability Equations," AIAA Paper 93-3053, 1993.

[40]Bertolotti, F. P., "Response of the Blasius Boundary-Layer to Free-Stream Vorticity," *Physics of Fluids*, Vol. 9, No. 8, 1997, pp. 2286–2299.

[41]Goldstein, M. E., and Wundrow, D. W., "On the Environmental Realizability of Algebraically Growing Disturbances and their Relation to Klebanoff Modes," *Theoretical and Computational Fluid Dynamics*, Vol. 10, No. 1–4, 1998, pp. 171–186.

[42]Breuer, K. S., and Haritonidis, J. H., "The Evolution of a Localized Disturbance in a Laminar Boundary Layer. Part 1. Weak Disturbances," *Journal of Fluid Mechanics*, Vol. 220, 1990, pp. 569–594.

[43]Blackwelder, R. F., "Analogies Between Transitional and Turbulent Boundary Layers," *Physics of Fluids*, Vol. 26, No. 10, 1983, pp. 2807–2815.

[44]Gad-el-Hak, M., and Hussain, F., "Coherent Structures in a Turbulent Boundary Layer. Part 1: Generation of "Artificial" Bursts," *Physics of Fluids*, Vol. 29, No. 7, 1986, pp. 2124–2139.

[45]Butler, K. M., and Farrell, B. F., "Optimal Perturbations and Streak Spacing in Wall-Bounded Turbulent Shear Flow," *Physics of Fluids*, Vol. 4, No. 3, 1993, pp. 774–777.

[46]Baig, M., and Chernyshenko, S. I., "Regeneration Mechanism of Streaks in Near-Wall Quasi-2D Turbulence," *European Journal of Mechanics B/Fluids*, Vol. 23, No. 5, 2004, pp. 727–736.

[47]Ali, R., "Receptivity and Transition in Boundary Layers over Rigid and Compliant Surfaces," Ph.D. Dissertation, School of Engineering, Univ. of Warwick, Coventry, England, March 2003.

[48]Lee, T., Fisher, M., and Schwarz, W., "Investigation of the Stable Interaction of a Passive Compliant Surface with a Turbulent Boundary Layer," *Journal of Fluid Mechanics*, Vol. 257, 1993, pp. 373–401.

[49]Johansson, A. V., Alfredsson, P. H., and Kim, J., "Evolution and Dynamics of Shear Layer Structure in near-Wall Turbulence," *Journal of Fluid Mechanics*, Vol. 224, 1991, pp. 579–599.

[50]Swearingen, J. D., and Blackwelder, R. F., "The Growth and Breakdown of Streamwise Vortices in the Presence of a Wall," *Journal of Fluid Mechanics*, Vol. 182, 1987, pp. 255–290.

[51]Gad-el-Hak, M., and Blackwelder, R., "Selective Suction for Controlling Bursting Events in a Boundary Layer," *AIAA Journal*, Vol. 27, No. 3, 1989, pp. 308–314.

[52]Lockerby, D. A., "Numerical Simulation of Boundary-Layer Control Using MEMS Actuation," Ph.D. Dissertation, School of Engineering, Univ. of Warwick, Coventry, England, U.K., March 2001.

C. Kaplan
Associate Editor